

## Distribution in angle of the Bloch correction in electronic stopping

Allan H. Sørensen

*Institute of Physics and Astronomy, University of Aarhus, DK-8000 Aarhus C, Denmark*

(Received 4 December 1996)

The position in angular space of the Bloch correction to the perturbative electronic stopping power formula of Bethe is investigated. It is demonstrated that this nonperturbative correction which originates in close collisions between the penetrating ion and target electrons appears at small scattering angles and that its position depends on the (adiabatic) cutoff at large distances. In the limit of infinite range the correction moves to infinitely small angles but remains finite and both the exact and the perturbative cross sections approach the Rutherford value at all finite angles. The picture is consistent with the lack of a Bloch-type correction in the energy-loss straggling. [S1050-2947(97)08504-1]

PACS number(s): 34.50.Bw, 34.80.-i, 03.65.Nk, 11.80.Et

### I. INTRODUCTION

When a charged particle penetrates matter at nonrelativistic though not excessively low speed, it loses energy essentially due to interaction with target electrons only. The stopping formula of Bethe [1] derived in first-order quantum perturbation theory is a standard reference for the average energy-loss rate experienced. It reads

$$-\frac{dE}{dx} = \frac{4\pi Z^2 e^4}{mv^2} nL \quad (1)$$

with the  $L$  factor defined as

$$L = \ln\left(\frac{2mv^2}{I}\right). \quad (2)$$

In Eqs. (1) and (2)  $Ze$  denotes the projectile charge,  $m$  is the electron mass,  $n$  the average electron density, while  $I$  is given in terms of dipole oscillator strengths  $f_{n0}$  and transition frequencies  $\omega_{n0}$  of the target medium of atomic number  $Z_2$  as  $\ln I = Z_2^{-1} \sum_n f_{n0} \ln(\hbar\omega_{n0})$ . The quantity  $v$  is the projectile speed, which here is assumed to be significantly higher than typical target electron velocities. The Bethe formula applies for moderate charge numbers  $Z$  at not too low velocities, more precisely, it applies when

$$\kappa = \frac{2Ze^2}{\hbar v} \ll 1; \quad (3)$$

see, for instance, the discussion given by Bohr [2].

Various corrections to the Bethe formula are in general to be considered. Of interest in this paper is the so-called Bloch correction [3], which accounts for the nonperturbative character of the interaction between the incoming particle and target electrons and which bridges the gap between the Bethe formula and Bohr's classical stopping formula [4], pertaining to large values of  $\kappa$ . It may be written as a correction  $\Delta L$  to Eq. (2) of

$$\begin{aligned} \Delta L &= -\text{Re}\psi(1+i\kappa/2) - \gamma \\ &= -\frac{\kappa^2}{4} \sum_{l=0}^{\infty} \frac{1}{(l+1)[(l+1)^2 + \kappa^2/4]} \end{aligned} \quad (4)$$

with  $\gamma$  and  $\psi$  denoting Euler's constant ( $\gamma=0.57721\dots$ ) and the logarithmic derivative of the gamma function, respectively. Other corrections include the so-called Barkas term and corrections for capture and loss of electrons, as well as for finite target electron motion.

The Bloch correction originates from close encounters between the penetrating charged particle and target electrons. In a recent paper [5], the deviation of the close-collision contribution to the stopping from the value predicted by quantum perturbation theory is examined for swift particles moving at arbitrary speeds. Although the emphasis in [5] is on the relativistic regime, the article is launched with a detailed discussion of the nonrelativistic case. This discussion is, in part, aimed at the clarification of a seeming paradox in Rutherford scattering, namely, that despite Rutherford scattering being valid both classically and in quantum theory (exact theory as well as first order perturbation), the Bloch correction may be extracted by simple operations which appear as simple angular integrations of differences in cross sections.

The purpose of the present paper is to supplement the discussion given in [5] of the above-mentioned apparent paradox. In particular, it will be demonstrated explicitly where in the angular spectrum the Bloch correction appears [6]. As a central point the dependence of the angular position of this close-collision correction on the (adiabatic) cutoff at large distances is exhibited, and it is shown how the appearance of the Bloch correction in stopping still is consistent with Rutherford scattering being valid independently of the value of the parameter  $\kappa$ . A few comments are included on the lack of a Bloch effect in straggling. Throughout, the discussion is restricted to the nonrelativistic case. Transcription to the relativistic case is straightforward by application of the formalism laid out in [5].

### II. FORMALISM

In [5] it is demonstrated that the requested correction  $\Delta L$  to the perturbative stopping logarithm (2) may be com-

puted as a difference in transport cross sections obtained in an exact and in a perturbative quantal calculation,

$$\Delta L = (\sigma_{\text{tr}} - \sigma_{\text{tr}}^{\text{pert}}) / (\pi \kappa^2 \lambda^2). \quad (5)$$

The transport cross sections, which belong to scattering of free electrons by the penetrating ion,  $\lambda = 2\pi\lambda$  being the wavelength of the relative motion, are obtained from the corresponding differential scattering cross sections  $d\sigma$  as

$$\sigma_{\text{tr}} = \int d\sigma (1 - \cos\theta), \quad (6)$$

where  $\theta$  denotes the scattering angle in the center-of-mass system; that is, essentially the electron scattering angle in the rest frame of the projectile (unless this itself is a very light particle). In a partial-wave analysis the integration over angles may be performed term by term to yield

$$\sigma_{\text{tr}} = 4\pi\lambda^2 \sum_{l=0}^{\infty} (l+1) \sin^2(\delta_l - \delta_{l+1}), \quad (7)$$

where  $\delta_l$  denotes the phase shift of the wave of angular momentum  $l\hbar$ .

With the Coulomb potential the sum (7) is divergent if extended to infinity. This holds true in the perturbative case (small  $\kappa$ ) as well as in the exact calculation (any  $\kappa$ ). However, by taking the difference between the two transport cross sections term by term before summation is performed the last expression in Eq. (4) emerges, and this is obviously convergent. It should be noted that the procedure of producing exactly this result by subtracting the two divergent sums relies on the fact that the adiabatic limit which determines the effective maximum value of the angular momentum essentially is independent of  $\kappa$ . Had this not been the case, then  $\Delta L$  would have contained an additional term essentially proportional to the sum of  $1/l$  between the two effective maximum  $l$  values, a number which of course could be large if the effective maxima were very different.

In the present analysis the aim is an investigation of the angular position of the Bloch correction, hence Eq. (7) and the results it produces will only be used for reference. Instead, we need an explicit expression for the differential cross section for electron scattering in a potential which is essentially coulombic out to a large distance where it is effectively cut off. As scattering potential, one may think of a Yukawa-type potential. However, if choosing so a Barkas correction will appear and this will to some extent obscure the analysis. To avoid the Barkas correction a Coulomb potential with a Gaussian screening function may be chosen, cf. [7]. A third alternative is to work directly with the Coulomb potential, compute the corresponding contributions to the scattering factor for the individual partial waves, and then introduce the cutoff by artificially diminishing contributions for high angular momenta. Although the Coulomb potential has its own problems this third alternative is chosen below since it is important to realize that the only ingredients needed in order to produce the Bloch correction are a Coulomb potential and a cutoff. Besides, this choice makes the numerical analysis quite simple.

The starting point is the same expression which lead to Eq. (7), namely,

$$\frac{d\sigma}{d\Omega} = |f(\theta)|^2, \quad (8)$$

where the scattering factor  $f(\theta)$  for the Coulomb potential is given as

$$f(\theta) = \frac{\lambda}{2i} \sum_{l=0}^{\infty} (2l+1) e^{2i\eta_l} P_l(\cos\theta); \quad (9)$$

cf. [8]. The phase shifts for the Coulomb case are the familiar

$$\eta_l = \arg\Gamma(l+1-i\kappa/2) = -\arg\Gamma(l+1+i\kappa/2). \quad (10)$$

It is exactly this simple form which, when applied in Eq. (7), allows a reduction to expression (4).

In order to obtain the perturbation value of the scattering cross section, an expansion of  $|f(\theta)|^2$  to second order in  $\kappa$  is needed. To this order, the phase shifts (10) reduce to

$$2\eta_l^{\text{pert}} = c_l \kappa, \quad c_l \equiv \gamma - \sum_{k=1}^l \frac{1}{k}, \quad (11)$$

with  $c_0 \equiv \gamma$ , and the perturbation value of the absolute square of the scattering factor reads

$$|f(\theta)|_{\text{pert}}^2 = (S_0^2 + S_1^2 - S_0 S_2) \lambda^2 / 4 \quad (12)$$

with the sums  $S_m$  defined as

$$S_m = \kappa^m \sum_{l=0}^{\infty} c_l^m (2l+1) P_l(\cos\theta), \quad m=0,1,2. \quad (13)$$

It may be noted, that besides the two terms proportional to  $\kappa^2$ , the perturbation result (12) contains one term, the first, which is independent of  $\kappa$ .

The difference  $|f(\theta)|^2 - |f(\theta)|_{\text{pert}}^2$  when integrated over angles with  $(1 - \cos\theta)$  and converted according to Eq. (5) reproduces the value of  $\Delta L$  given in Eq. (4). And since convergence of the integrated difference with increasing  $l$  is fast with terms essentially decreasing as  $l^{-3}$ , only relatively few partial waves are needed to obtain a high precision. However, as far as  $|f(\theta)|^2$  and  $|f(\theta)|_{\text{pert}}^2$  are concerned individually, the situation is completely different. The sums for  $f$  are simply divergent. If summed up to a maximum  $l$  value of  $l_{\text{max}}$ , the absolute squares oscillate with increasing amplitude and increasing number of zero points as  $l_{\text{max}}$  is increased. It may also be noted, that for any fixed value of  $\kappa$ , however small, the Coulomb phase shifts become large at sufficiently large values of  $l$ , cf. Eqs. (10) and (11). The Rutherford cross section is never approached. The situation is clearly illustrated by the value of the stopping logarithm  $L'$  obtained by integrating  $(1 - \cos\theta)|f(\theta)|^2$  over angles and converting according to Eq. (5),

$$L' = \frac{l_{\text{max}} + 1}{\kappa^2} + \sum_{l=0}^{l_{\text{max}}-1} \frac{l+1}{(l+1)^2 + \kappa^2/4}. \quad (14)$$

While the second term on the right-hand side is the term that remains for unrestricted summation (with  $l_{\text{max}}$  tending to infinity), the first term remains due to lack of the compensating

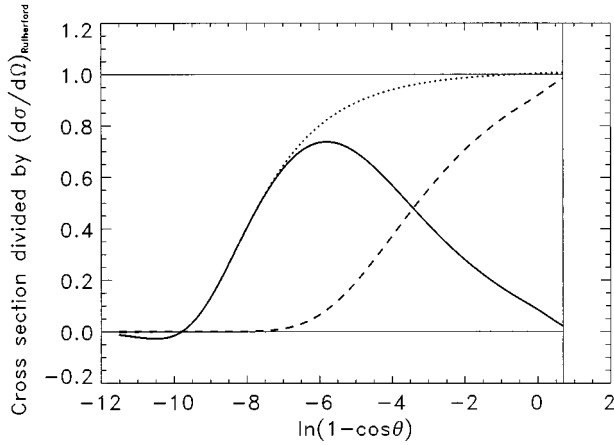


FIG. 1. Differential cross sections for finite value of  $1-X$ . All cross sections are given in units of the Rutherford value at any given angle and shown as functions of  $\ln(1-\cos\theta)$ , where  $\theta$  denotes the scattering angle. The dashed curve corresponds to  $|f_X(\theta)|^2$ , the dotted to  $|f_X(\theta)|_{\text{pert}}^2$ , and the full-drawn curve displays the difference  $|f_X(\theta)|_{\text{pert}}^2 - |f_X(\theta)|^2$ . The projectile atomic number is  $Z=92$  and the convergence parameter attains the value  $X=0.99$ . The kinetic energy of the electron in the rest frame of the ion is  $0.01mc^2$ , i.e., the kinetic energy of the ion in the laboratory is 9.3 MeV/amu.

term, which in the unrestricted summation appears for  $l=l_{\text{max}}+1$ . Obviously, the first term becomes large for large  $l_{\text{max}}$ , in particular if  $\kappa$  is small.

Although divergent, the series for  $f$  is summable as the limit of a power series on its radius of convergence. This has been discussed and utilized by Mott in the relativistic case for a different purpose, cf. [9]. We shall adopt the procedure here in order to mimic an effective cutoff at some large  $l$  value and hence in place of  $f$  use

$$f_X(\theta) = \frac{\chi}{2i} \sum_{l=0}^{\infty} (2l+1) X^l e^{2i\eta_l} P_l(\cos\theta), \quad (15)$$

where the convergence parameter  $X$  is a number which is slightly less than 1. The corresponding perturbation value is still given by Eqs. (12) and (13) except for a factor of  $X^l$  to be included in each of the sums  $S_m$ . It may be noted, that in the limit  $X \rightarrow 1^-$  the sum  $S_0$  vanishes for any nonzero angle; see also [8]. It may further be noted that for any finite value of  $1-X$  the sum (4) giving the Bloch correction should include a factor of  $X^{2l}$ .

### III. NUMERICAL RESULTS

Figure 1 displays  $|f_X(\theta)|_{\text{pert}}^2$  and  $|f_X(\theta)|^2$  as well as their difference, all in units of the Rutherford cross section

$$(d\sigma/d\Omega)_{\text{Rutherford}} = (\chi^2/4)\kappa^2/(1-\cos\theta)^2, \quad (16)$$

as functions of  $\ln(1-\cos\theta)$  for a standard heavy-ion case. The convergence parameter is chosen to be  $X=0.99$ , and summation is performed up to a large  $l$  value (10 000) in order to ensure convergence at all angles. Scattering into the backward hemisphere corresponds to positive values of the

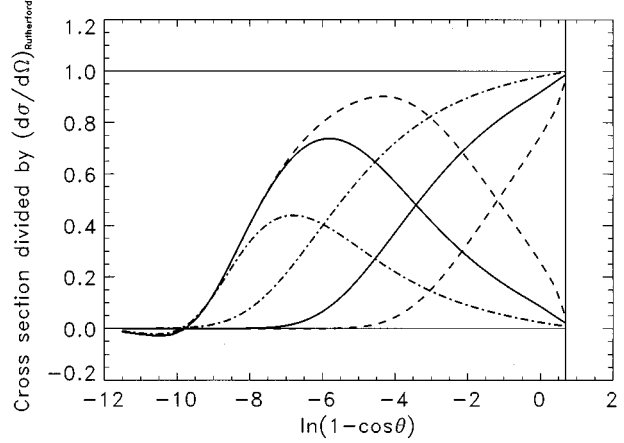


FIG. 2. Variation of differential cross sections with primary energy for a heavy ion,  $Z=92$ . The three curves starting out at maximum value for backward scattering display  $|f_X(\theta)|^2$  while the three remaining curves show the difference function  $|f_X(\theta)|_{\text{pert}}^2 - |f_X(\theta)|^2$ . The value of the convergence parameter is 0.99 and the kinetic energies of the electron in the rest frame of the ion are  $0.001mc^2$  (dashed curves),  $0.01mc^2$  (full drawn), and  $0.1mc^2$  (chained curves) corresponding to ion kinetic energies in the laboratory of 0.93, 9.3, and 93 MeV/amu. The corresponding values of the parameter  $\kappa$  are 30, 9.6, and 3.2. Axes and units are as in Fig. 1.

abscissa (the interval from 0 to the maximum of  $\ln 2$ ), while forward scattering corresponds to negative values. The finite value of  $1-X$  implies a cutoff at small angles, while at larger angles the Rutherford cross section is approached. Starting in the wide-angle scattering region, the cutoff appears earlier (i.e., at larger angles) for the exact case than for the perturbative case. The difference between the two peaks at rather small angles. With the abscissa chosen as  $\ln(1-\cos\theta)$  the area under the difference curve gives directly  $-2\Delta L$ , hence obviously the Bloch correction, which originates in close collisions (small  $l$ ), appears at small angles.

The variation of the cross section  $|f_X(\theta)|^2$  and the difference  $|f_X(\theta)|_{\text{pert}}^2 - |f_X(\theta)|^2$  with primary energy is illustrated in Fig. 2 for a high atomic number and in Fig. 3 for a low atomic number. As the energy is increased, the difference

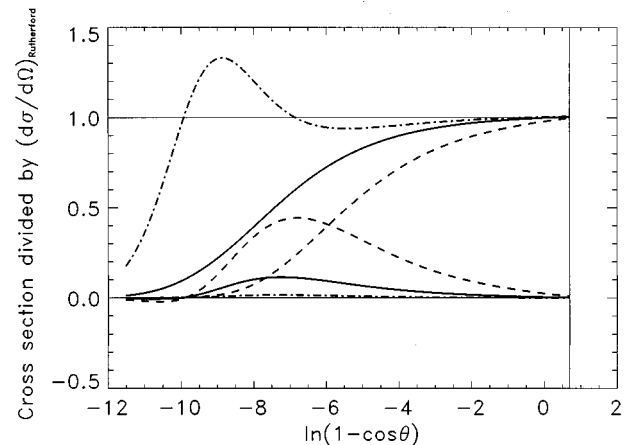


FIG. 3. As Fig. 2 but for a light ion,  $Z=10$ . The parameter  $\kappa$  attains the values 3.3, 1.0, and 0.35 in the three cases.

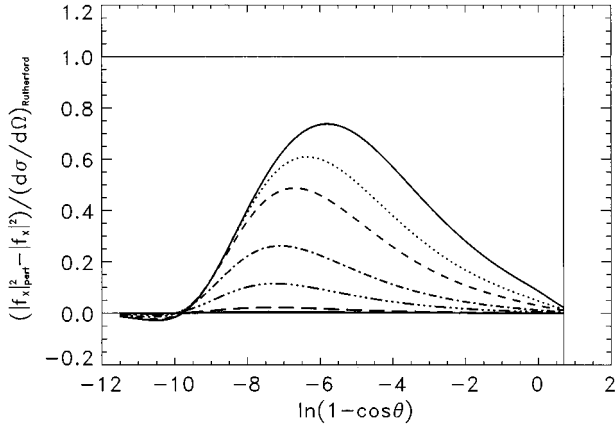


FIG. 4. Variation of difference cross section  $|f_X(\theta)_{\text{pert}}|^2 - |f_X(\theta)|^2$  with projectile atomic number. The value of the convergence parameter is 0.99 and the kinetic energy of the electron in the rest frame of the ion is  $0.01mc^2$ , i.e., the kinetic energy of the ion in the laboratory is 9.3 MeV/amu. The charge numbers are 92 (upper full-drawn curve), 54 (dotted), 36 (dashed), 18 (chained), 10 (triple-dotted-dashed), 4 (long dashes), and 2 (full-drawn curve near 0.0 at all angles). Axes and units are as in Fig. 1.

function becomes smaller, yielding a lower value of  $-\Delta L$ , and Rutherford scattering holds to smaller angles. Note that increasing energy implies decreasing value of the parameter  $\kappa$ , cf. Eq. (3). For the high charge, the perturbation value closely follows that displayed in Fig. 1 at all three energies. For the low charge, on the other hand, the perturbation cross section develops a peak structure at the highest energy closely resembling the structure of the exact cross section at this energy (the difference curve attaining low values at high energies). The appearance of the peak will be discussed further below. Although a comparison with experiments is not the aim of the current investigation a warning should be issued before the discussion of Figs. 2 and 3 is closed: At the highest energy, relativistic corrections, which are not included in the present study, are important; for the higher of the two charges they reduce the value of  $\Delta L$  to roughly half of the nonrelativistic value and for the lower of the two charges they closely balance the nonrelativistic result to yield a  $\Delta L$  which nearly vanishes, cf. [5]. At the lower energies the heavier ion will carry electrons and additional corrections apply. Besides, in a study of stopping powers, shell corrections (finite electron velocities) and the Barkas correction should be included.

The variation with projectile atomic number at fixed energy is demonstrated by Figs. 4 and 5. The difference function, Fig. 4, is seen to be concentrated in the same angular region for all  $Z$  values with a slight drift towards larger angles for large  $\kappa$ . The exact cross section, Fig. 5, is again seen to follow the Rutherford law closely to still lower angles as the value of  $\kappa$  is decreased. For very small charge numbers (small  $\kappa$ ) a peak structure similar to that seen in Fig. 3 at the highest energy appears in the exact cross section. On a plot similar to Fig. 5, the perturbation cross sections are hardly distinguishable for the three higher charge numbers (36, 54, and 92), whereas for lower charge numbers differences appear with the peak structure developing for the two lowest charges displayed (4 and 2). If the energy is

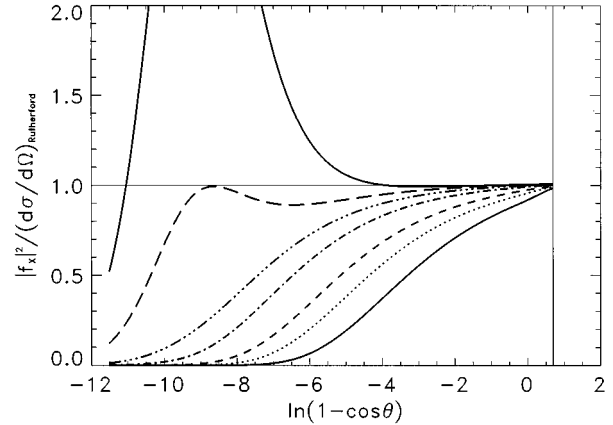


FIG. 5. As Fig. 4 but displaying the exact cross section  $|f_X(\theta)|^2$ . The lowest full-drawn curve is for  $Z=92$ . The upper solid line, which applies for  $Z=2$ , peaks with a maximum of 3.55.

decreased by a factor of 10, only the perturbation curves for the two lowest charge numbers separate from the rest, but in this case without developing a peak.

All the numerical results discussed above were obtained for the same value of the convergence parameter  $X$ , namely,  $1-X=0.01$ . The introduction of the convergence parameter in Eq. (15) mimics an effective cutoff at some large  $l$  value, and the lower the value of  $1-X$  the higher is the effective maximum  $l$ . A major point of this investigation is to demonstrate how the angular spectrum is influenced by the cutoff and, in particular, to see how the close-collision Bloch correction moves about in angular space as the long distance interaction is altered. Furthermore, it is the aim to demonstrate that the appearance of the Bloch correction does not prevent differential cross sections, both perturbative and exact ones, to approach the Rutherford value. Hence, the variation with the convergence parameter  $X$  is to be exploited next.

Figure 6 demonstrates the variation of the difference function  $|f_X(\theta)_{\text{pert}}|^2 - |f_X(\theta)|^2$ ; that is, the variation of the Bloch correction as  $1-X$  varies between 0.016 and 0.001. What is immediately apparent is that the correction moves left; that is to smaller angles, as  $1-X$  decreases. The shape of the curve is essentially the same in all cases, only small changes appear due to the cutoff of the wide-angle scattering tail for the higher values of  $1-X$  [this is reflected in a slight variation of  $\Delta L$  of Eq. (4) when a factor of  $X^{2l}$  is included]. For the considered heavy-ion case, the maximum of the difference curve appears at angles of  $\approx 7.8(1-X)$ ; that is, it varies between  $7^\circ$  and  $0.4^\circ$  in Fig. 6. So, what the figure demonstrates explicitly is that the close-collision Bloch correction is always present some place in angular space when an effective cutoff at large distances is introduced. The correction just wanders around, its position depending on how far out the effective cutoff appears, such that increasing range implies migration towards smaller angles.

As the Bloch correction moves to smaller angles with decreasing value of  $1-X$  and otherwise remains undisturbed, Fig. 6, the cross section  $|f_X(\theta)|^2$  approaches the Rutherford value over an increasing range of angles starting in the wide-angle scattering domain. This is demonstrated in Fig. 7, which shows the exact cross section for the same case

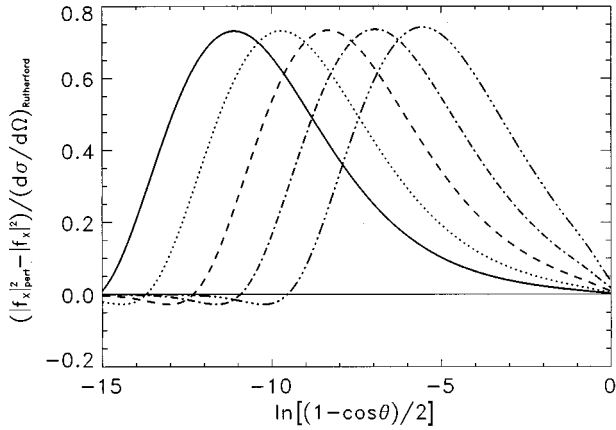


FIG. 6. Variation of difference cross section  $|f_X(\theta)|_{\text{pert}}^2 - |f_X(\theta)|^2$  with the convergence parameter. The cross section is given in units of the Rutherford value and shown as a function of  $\ln[(1-\cos\theta)/2]$ . Backward scattering corresponds to values of the abscissa varying between  $-\ln 2$  and 0. The values of  $1-X$  are 0.001 (solid curve), 0.002 (dotted curve), 0.004 (dashed), 0.008 (chained), and 0.016 (triple-dotted-dashed). The projectile atomic number is  $Z=92$  and the kinetic energy of the electron in the rest frame of the ion attains the value  $0.01mc^2$ , i.e., the kinetic energy of the ion in the laboratory is 9.3 MeV/amu. The maximum  $l$  value is chosen to be 100 000 except for  $1-X=0.016$ , where 10 000 suffices.

and  $X$  values as in Fig. 6. Hence, when the effective cutoff is increased ( $1-X$  decreased), the Rutherford value applies way down to small angles. In the limit  $X \rightarrow 1^-$  the Bloch correction has moved to zero angle, and the Rutherford cross section is found at all finite angles.

While the main point of this investigation is illustrated by Fig. 1 and, in particular, Figs. 6 and 7, the behavior of the perturbative cross section  $|f_X(\theta)|_{\text{pert}}^2$  also deserves a few words. Figure 8 displays the variation of the ingredients  $(1-\cos\theta)^2 S_0^2$  and  $(1-\cos\theta)^2 (S_1^2 - S_0 S_2)/\kappa^2$  with angle for two different values of  $X$ . The sums  $S_m$  are given by Eq. (13) with a factor of  $X^l$  included on each term. The plotted quantities are universal insofar as they do not depend on the projectile and the chained curve plus the full drawn divided by

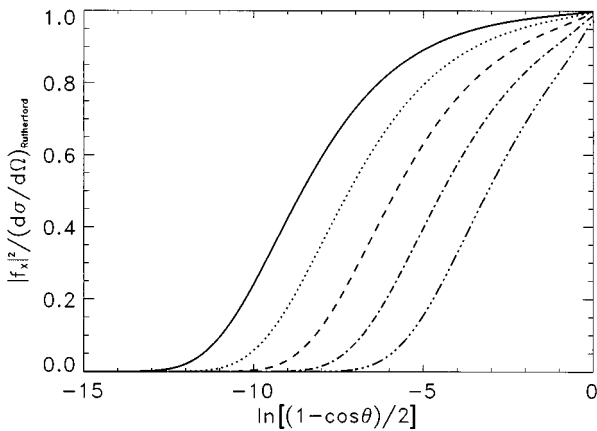


FIG. 7. As Fig. 6 but displaying the exact cross section  $|f_X(\theta)|^2$ .

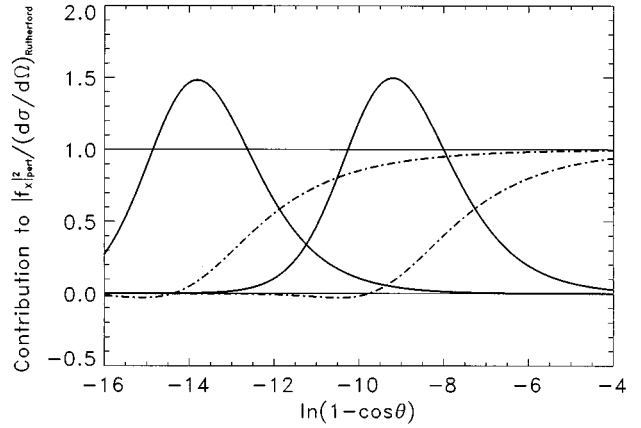


FIG. 8. Contributions to the perturbative cross section at two different values of  $X$ . The solid curves display  $(1-\cos\theta)^2 S_0^2$  and the chained curves show  $(1-\cos\theta)^2 (S_1^2 - S_0 S_2)/\kappa^2$ ; cf. text for details. The solid curve showing maximum at the lowest angle and the chained curve showing a cutoff at the lowest angle are computed for  $X=0.999$  while the remaining curves are for  $X=0.99$ . The abscissa is chosen as in Fig. 1 and the quantities plotted are dimensionless.

$\kappa^2$  make up  $|f_X(\theta)|_{\text{pert}}^2$  in units of the Rutherford cross section, cf. Eqs. (12) and (16). For high values of  $\kappa$  the monotonic curves obviously dominate, and we encounter essentially the Rutherford value down to a small  $X$ -dependent cutoff angle (considerably smaller than the cutoff angle for the exact case). For low values of  $\kappa$ , the peak, which was evident in Figs. 3 and 5, develops. The  $S_0^2$  peak moves with  $1-X$  with essentially undisturbed shape much like the Bloch correction, Fig. 6, and in the limit  $X \rightarrow 1^-$  its contribution is zero at all finite angles. In this limit, Fig. 8 clearly demonstrates that the perturbative cross section equals the Rutherford value at all finite angles.

#### IV. CONCLUDING REMARKS

No correction similar to the Bloch correction appears in the average square fluctuation in energy loss, cf. [5]. To get the straggling, the differential cross sections should be multiplied by  $(1-\cos\theta)^2$  rather than just by  $1-\cos\theta$ . Indeed, if the exact and perturbative cross sections are computed according to Eqs. (8) and (9), respectively, and (12) and (13), then the difference between the straggling contributions essentially vanishes already for modest values of the maximum  $l$  value applied in the summation. It is easy to see how the lack of a Bloch-type correction in straggling fits with the angular distributions displayed above. To get such correction, the difference curves should be multiplied by  $1-\cos\theta$  before integration. However, as difference curves peak in the region of very low values of this factor, and as the difference curve furthermore moves to even smaller angles as the value of  $1-X$  is increased, the resulting correction vanishes in the limit  $X \rightarrow 1^-$ .

#### ACKNOWLEDGMENT

The present work was supported by the Danish Natural Science Research Council.

- [1] H. A. Bethe, *Ann. Phys. (Leipzig)* **5**, 325 (1930).
- [2] N. Bohr, *K. Dan. Vidensk. Selsk. Mat. Fys. Medd.* **18**, No. 8 (1948).
- [3] F. Bloch, *Ann. Phys. (Leipzig)* **16**, 285 (1933).
- [4] N. Bohr, *Philos. Mag.* **25**, 10 (1913).
- [5] J. Lindhard and A. H. Sørensen, *Phys. Rev. A* **53**, 2443 (1996).
- [6] From Bloch's original paper [3] it is possible to extract that the correction (4) appears at small scattering angles in close collisions. This result, which may seem surprising at first, is confirmed in Sec. III through application of a much simpler analysis than that originally given by Bloch.
- [7] J. Lindhard, *Nucl. Instrum. Methods* **132**, 1 (1976).
- [8] L. I. Schiff, *Quantum Mechanics* (McGraw-Hill Kogakusha, Tokyo, 1968).
- [9] N. F. Mott, *Proc. R. Soc. London Ser. A* **124**, 425 (1929); **135**, 429 (1932).